Grain growth in weak electric fields in strontium titanate: grain growth acceleration by defect redistribution

Wolfgang Rheinheimer*, Manuel Fülling and Michael J. Hoffmann

Institute of Applied Materials – Ceramic Materials and Technologies, Karlsruhe Institute of Technology, Karlsruhe, Germany

*wolfgang.rheinheimer@kit.edu, +49 721 608 47922

Abstract

The impact of DC electric fields on grain growth in strontium titanate is investigated between 1350°C and 1550°C for fields of up to 50 V/mm. To prevent joule heating by electrical currents, insulating Al_2O_3 plates separate electrodes from samples. The seeded polycrystal technique is used, which allows evaluating gradients induced by electric fields. The growth direction of the single crystalline seeds is perpendicular to the electric field; hence electrostatic forces do not influence its growth. Below 1425°C, the influence of electric fields is very weak. Above 1425°C the field results in an increase of the grain boundary mobility at the negative electrode.

The enhancement of the boundary mobility at the negative electrode is attributed to electric field induced defect redistribution. Oxygen vacancies migrate towards the negative electrode, while strontium vacancies accumulate at the positive electrode. This defect redistribution is connected to the defect chemistry dependent grain growth in strontium titanate.

Keywords: field assisted grain growth; defects; grain boundary mobility, strontium titanate; grain growth anomaly

1. Introduction

Within the last five years considerable efforts were expend in understanding electric field assisted sintering (flash sintering). Flash sintering refers to accelerated sintering in electric fields [1, 2]. This method involves high currents flowing through the sample and thereby joule heating. Different ceramic materials show this effect, for example alumina [3], silicon carbide [4], zirconia [1, 5-9], barium titanate [10] and strontium titanate [11]. The mechanism of flash sintering is under debate. While most likely joule heating is involved [12-

14], different defect based mechanisms were proposed as well [1, 2, 5, 15]. Further experimental and theoretical work is ongoing in a multitude of working groups.

However, flash sintering experiments are very hard to control: shrinkage occurs within seconds and the local temperature is undefined due to joule heating. Analyzing grain growth in an electric field simplifies these experiments and provides information on the active mechanisms. Only, few studies focused on the impact of electric fields on grain growth. In experiments with an electric current flow and joule heating in zirconia, a suppression of grain growth with electric fields of up to 40 V/mm was found [1, 16, 17]. The authors explained the observations by a reduction of the grain boundary entropy and energy by local joule heating of the interfaces and local point defect creation. These point defects are believed to segregate and to cause a solute drag-like [18] effect on boundary motion.

Two similar studies have investigated grain growth in barium titanate in an electric field of 20 V/mm at different dopant concentrations and atmospheres [19, 20]. The authors report diverse growth gradients across the samples depending on dopant concentration and atmosphere. Several complex grain growth effects seem to be coupled, for example a change of the boundary potential from positive (acceptor doped and undoped) to negative (donor doped) and a field induced wetting transition. Wetting is assumed to increase the boundary mobility drastically. The authors explain all growth effects observed in the samples by the grain boundary potential and its interaction with local defect concentrations, which are graded across the sample due to the electric field. However, the composition of the second phase, joule heating, a possible change in faceting and its impact of grain growth [21-24] are not considered.

At these fields, joule heating is expected due to the high conductivity of these materials at high temperature. Accordingly, the present study focuses on grain growth in the no-current case with insulating alumina plates to separate the electrodes from the samples. The seeded polycrystal method was used, in which a single crystal is joined to a polycrystalline matrix [25, 26]. This method allows evaluating the grain boundary mobility continuously across the sample and highlighting gradients induced by the electric field. In alumina [27] and sodium chloride [28], the general impact of electrostatic forces on grain boundary migration parallel to electric fields was documented. Thus in the present experiments the growth direction of single crystalline seeds was orthogonal to the electric field to prevent possible effects. The perovskite model system strontium titanate was chosen, since its grain growth behavior is

well-known in relation to defect chemical parameters (but in the absence of electric fields). For example a grain growth transition was documented resulting in strongly decreasing grain growth rates with increasing temperature [29-31]. Information on grain boundary energy [32, 33] and mobility anisotropy [25, 26] as well as grain boundary faceting [34-36] and atomic structure [37] are available. The impact of stoichiometry on grain growth was thoroughly examined [31, 38, 39] and the bulk defect chemistry is well-known [40, 41].

2. Experimental Procedure

Stoichiometric strontium titanate powder was prepared by the mixed oxide/carbonate route based on high purity raw materials ($SrCO_3$ and TiO_2, both 99.9+%, Sigma Aldrich Chemie GmbH, Taufkirchen, Germany). The green bodies were sintered at 1425 °C for 1 h in oxygen to a relative density of 99.5 ± 0.2 %. Further details of the powder synthesis are published elsewhere [42]. Samples were cut into discs and polished (diamond slurry, 0.25 µm) and then scratched with a polishing disc (30 µm diamonds) to create pore channels. These pore channels mark the original position of the interface during growth experiments (cf. white broken line in Figure 1 a and c [26, 33]).

The seeded polycrystal technique was used to evaluate the impact of an electric field on grain growth. A single crystalline disc (chemical-mechanical polished, impurity content: <10 ppm Si, <2 ppm Ba, <1 ppm Ca, SurfaceNet GmbH, Rheine, Germany) was placed between two polycrystalline discs and joined by a diffusion bonding process (1430°C, 20 min in air, 1 MPa). A typical microstructure of a seeded polycrystal is shown in Figure 1c. The single crystal grows into the polycrystal. The driving force for this growth is the interface area of the polycrystal consumed by the growing single crystal. Further details on this experimental setup are published elsewhere [26, 33].

Samples were again cut perpendicular to the single crystal in slices of a thickness of about 2 mm. As shown in Figure 1b, samples were placed between two high purity alumina plates (thickness of 1 mm) to avoid joule heating by a current flowing through the sample. To prevent any reaction of strontium titanate with alumina, a very thin layer (<0.1 mm) of coarse zirconia powder was spread in the contact area to prevent any direct contact. No influence or reaction of the zirconia on the strontium titanate was found.

On top of both alumina plates platinum sheets were used as electrodes. These sheets were contacted with platinum wires, which were passed outside the furnace to a voltage source

(XG 600-2.8, AMETEK, San Diego, USA). The applied fields were 25 V/mm and 50 V/mm. Voltage and current were measured and logged (Type GL200A, Graphtec Corp., Yokohama, Japan); no current was detectable for all experiments due to the insulating alumina plates. Grain growth experiments were done in a batch furnace between 1350°C and 1550°C in air (Gero GmbH, Neuhausen, Germany).

The mean grain radius was obtained by the line intersection method on SEM micrographs. Due to the microstructural gradient for every sample three different positions were observed (at both electrodes and in the middle of the sample). For each measurement typically 200 grains were counted (min. 120). The growth front of the single crystal was documented across the entire sample by assembling 5-10 SEM images (Figure 1c).

In these assembled images the growth length was measured in every pixel and plotted (thin line in Figure 1d). Additionally the data was fitted with a polynomial of second degree to highlight the trend of the growth length (thick line in Figure 1d).

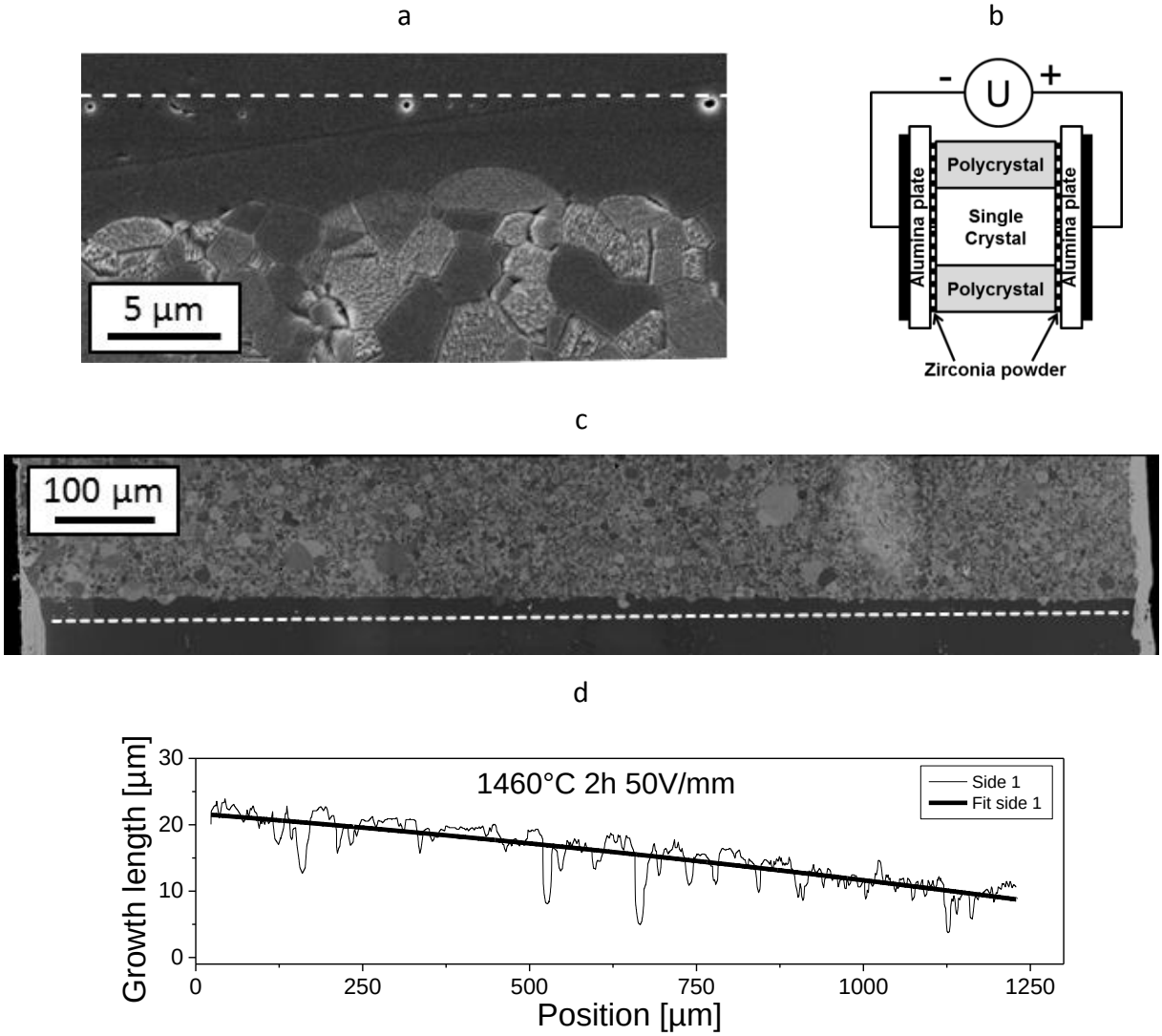

Figure 1: Microstructure of a seeded polycrystal after diffusion bonding (a). The initial position of the interface prior to bonding is marked by a row of small pores (white broken line). Sketch of the experimental setup with seeded polycrystal, insulating alumina plates and voltage source (b). Microstructure across a sample from negative (left side) to positive electrode (right side) after 2 h at 1460°C and 50 V/mm (c). The initial position of the interface prior to bonding is marked by a row of small pores (white broken line). The growth length between the initial and actual position is shown in d with respect to the position in the sample (d).

3. Results and Discussion

3.1. True external electric field in the chosen experimental setup

Due to the experimental setup using insulating alumina plates, the true field distribution in the sample should be addressed. Not the entire potential is applied at the sample; the experimental setup can be understood as a set of capacitors in series (Figure 2a and b). In the following, the capacity of the two insulating alumina plates $C_{i,1}$ and $C_{i,2}$ is combined to a

single capacity C_i (Figure 2c). For this situation, the following equation can be obtained (see appendix for derivation)

$$\frac{E_{sample}}{E_{tot}} = \frac{d_s + d_i}{d_s\left(1 + \frac{\epsilon_{r,STO} d_i}{\epsilon_{r,alumina} d_s}\right)} \qquad 1$$

with the electric field at the sample E_s, the overall electric field E_{total}, the sample and insulator thickness d_s and d_i and the relative permittivity of strontium titanate $\epsilon_{r,STO}$ and alumina $\epsilon_{r,alumina}$. In the present experiment, we can assume [43, 44]

$$d_s = 2mm,\ d_i = 2mm,\ \epsilon_{r,STO}^{1400°C} \approx 55\ and\ \epsilon_{r,alumina}^{1400°C} \approx 20 \qquad 2$$

to estimate the true electric field in the sample:

$$\frac{E_s}{E_{total}} \approx 0.53 \qquad 3$$

Thus, in the present experiments the true electric field at the sample is lowered significantly by the insulating alumina plates at the electrodes (13.25 V/mm instead of 25 V/mm and 26.5 V/mm instead of 50 V/mm). The thin layer of zirconia powder (Figure 1b) may result in an additional reduction of the field: If we assume a powder layer thickness of 0.1 mm and a tentative dielectric constant of 5, we may lose another ~30% of the electric field according to Eqn. 1. Nevertheless, since this is just a rough estimation (e.g. the relative permittivity at high temperatures are uncertain), we used the overall electric fields in the discussion.

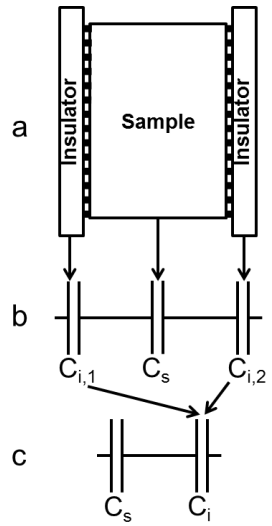

Figure 2: Derivation of an equivalent circuit to estimate the true electric field across the sample. The sample and both insulators at the electrode (a) are assumed to represent capacitors with the capacity $C_{i,1}$, $C_{i,2}$ and C_s (b). $C_{i,1}$, $C_{i,2}$ can be combined to a single capacity $C_{i\,(c)}$.

3.2. Microstructure

The microstructures of all samples are shown in Figure 3 (three images refer to the microstructure near the negative electrode, in the center of the sample and near the positive electrode). The microstructures are unimodal at 1350°C and 1550°C and bimodal at 1425°C and 1460°C as expected for strontium titanate [26, 30, 45, 46]. No elongated or grain shapes could be found in the 2D cross sections in Figure 3; accordingly the electric field does not seem to generate a significant grain shape texture. Up to 1425°C (Figure 3a-d), no significant change of the microstructure from the negative to the positive side appears. Above 1460°C (Figure 3e-h) a gradient of the grain size develops: At the negative electrode the grain size is largest and at the positive electrode the grain size is smallest. In the center of the sample, the grain size is between these two extremes. This effect is stronger at higher electric fields (Figure 3 f and h).

During the experiments the single crystals grow into the polycrystal. This effect was described elsewhere in detail and gives a simple approach to the grain boundary mobility [26]. In general, it can be shown that the single crystal exhibits the same growth behavior (i.e. grain boundary mobility) as polycrystals [25, 26]. Therefore, the growth length of all samples shows no gradient below 1425°C (Figure 3a-d). For 1460°C and 50 V/mm (Figure 3f) as well as for 1550°C (Figure 3g and h) a gradient appears similar to the grain size with the highest growth lengths at the negative electrode and the shortest at the positive electrode. However, at 1460°C and 25 V/mm no gradient of the growth length was found, although the grain size clearly shows a gradient. This is more obvious in the data shown in section 3.1.

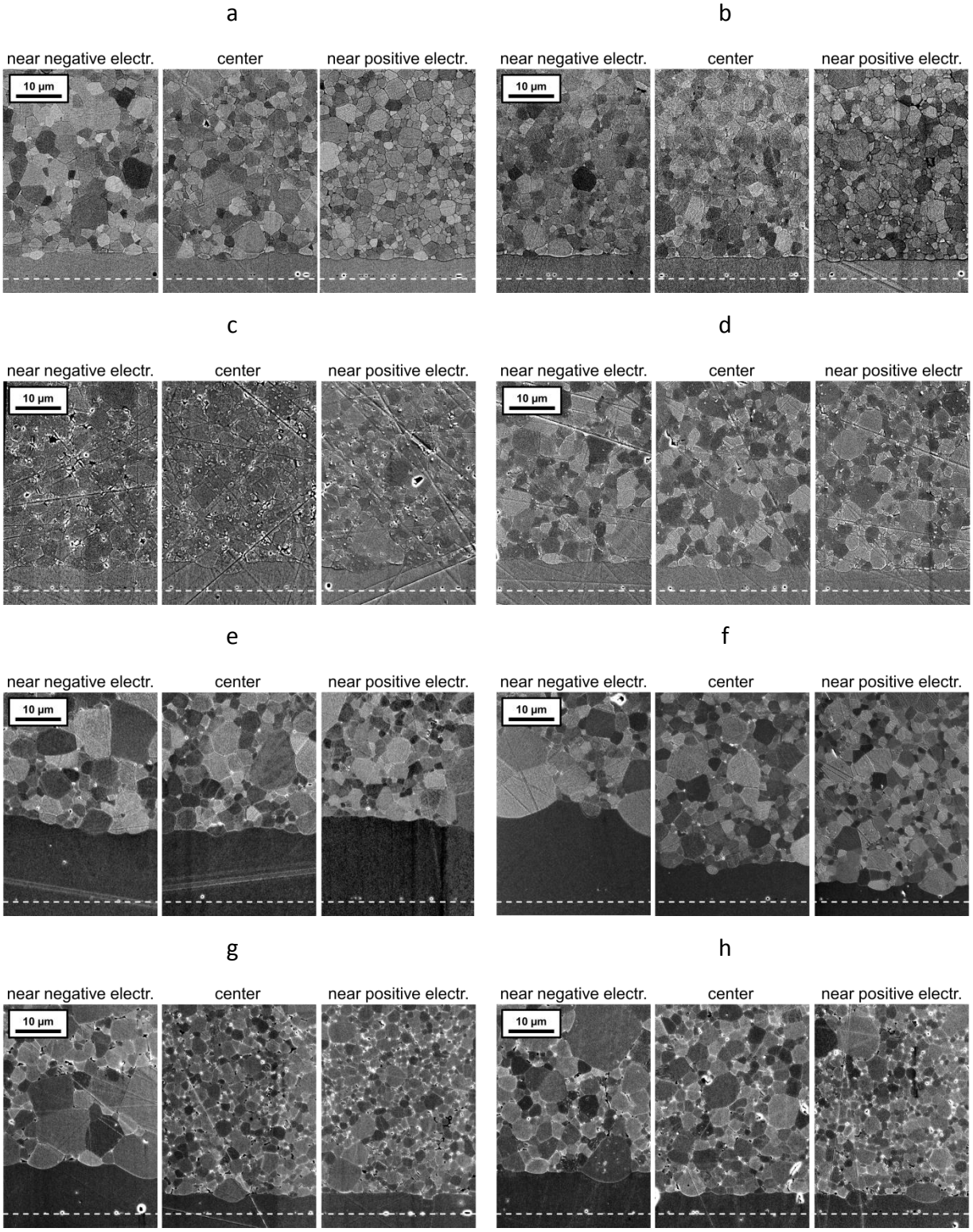

Figure 3: Microstructures of the seeded polycrystals after 10 h at 1350°C (a, b), after 10 h at 1425°C (c, d), after 2 h at 1460°C (e, f) and after 30 min at 1550°C (g, h). The electric field was 25 V/mm (a, c, e and g) and 50 V/mm (b, d, f and h). The original interface between polycrystal and single crystal is highlighted by a dashed line. Every set of images gives microstructures at the negative electrode (left), in the middle of the sample (middle) and at the positive electrode (right).

3.3. Growth of single crystalline seeds

Figure 4 quantifies the growth effects described in section 5. The graphs give the growth length of the single crystal with respect to the position in the sample; additionally a fitted line highlights the trend of the growth length. In principle, the experimental setup (Figure 1b) provides two growth fronts of the single crystal. However, due to the complexity of the experimental setup and sample preparation several samples were damaged; samples tend to cleave along the interface of the single crystal. Thus for some samples only one growth front could be examined (Figure 4e, f and h). For two samples only parts of the interface broke and some data is missing (Figure 4a, side 1 left and Figure 4d, side 2 left), but the position of the curves was corrected to ensure comparability with the second side of the sample.

As in Figure 3, no significant effect of the electric field appears at 1350°C and 1425°C at 25 V/mm (Figure 4a-c). At 1425°C and 50 V/mm, a slight gradient is evident with faster growth at the negative electrode. At 1460°C and 50 V/mm (Figure 4f) and at 1550°C (Figure 4g and h) a strong gradient with much larger growth lengths at the negative electrode is visible. At 1550°C and 50 V/mm, the positive electrode reveals a plateau with small growth lengths.

The position dependent mean grain size was added to the graphs in Figure 4 and shows the same behavior as the growth length with one exception at 1460°C where the ratio of growth length to mean grain size is higher compared to other temperatures. This effect is well-known and seems to be related to exaggerated growth of the single crystalline seeds at this particular temperature [26]. The growth front of the single crystal also shows a pronounced scattering, which is caused by a macroscopic waviness of the interface between polycrystal and single crystal (cf. Figure 3 [26]). At 1460°C this scattering is strongest as microstructures are bimodal.

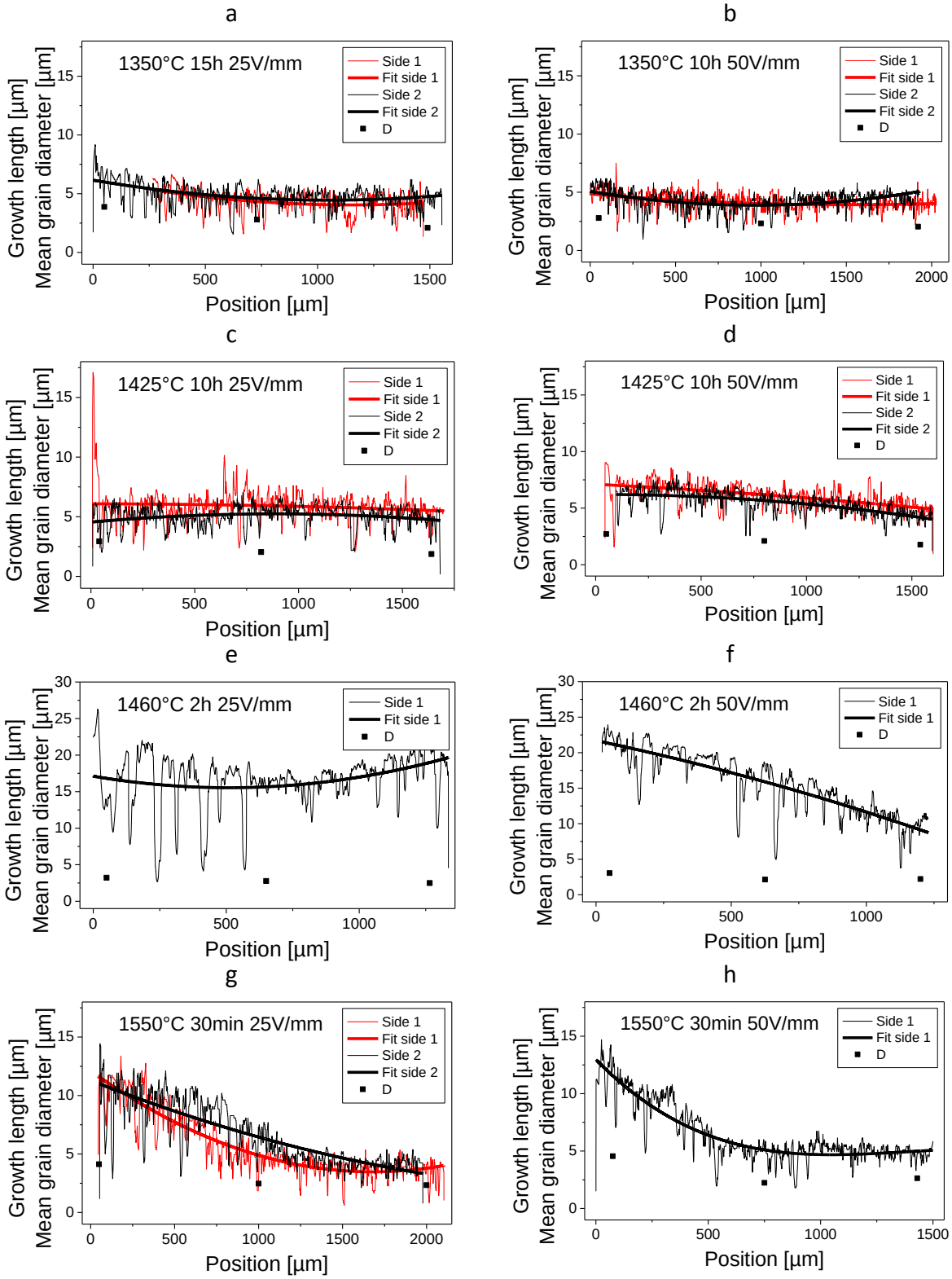

Figure 4: Measured growth length of the single crystals after 10 h at 1350°C (a, b), after 10 h at 1425°C (c, d), after 2 h at 1460°C (e, f) and after 30 min at 1550°C (g, h). The electric field was 25 V/mm (a, c, e and g) and 50 V/mm (b, d, f and h). The negative electrode was on the left side (and the positive electrode on the right side). The mean grain size was added to the graphs. For most samples two datasets are given according to the two sides of the single crystals. In two cases (side 1 in a and side 2 in d) some data is missing due to breakout during polishing. The thick lines represent a fitted polynomial of second degree to highlight the trend of the growth length.

3.4. Growth of polycrystals

The grain sizes given in Figure 4 can be used to compare grain growth to literature data (Figure 5 [30]) using the standard grain growth equation [47]

$$D^2 - D_0^2 = kt \qquad 4$$

with the mean grain size D, the mean initial grain size D_0 at time t = 0 and the grain growth constant k. The present dataset allow only estimating the grain growth constant on a very rough scale, since only one heating time was done for each experiment. For this estimation D_0 was assumed as the mean powder particle size of 0.3 µm [45]. The obtained data is plotted in Figure 5 along with literature data [30, 31]. Strontium titanate is known to show a grain growth transition within the temperature range from 1350°C to 1425°C indicating non-Arrhenius behavior of the grain growth constant. In general, the estimated grain growth constants fit the literature data very well. At 1550°C and at 1350°C the estimated k is lower than expected and at 1350°C the two samples (25 V/mm and 50 V/mm) differ slightly as well, but given the uncertainty in k due to the estimations the accordance is still sufficient.

For all temperatures, k is higher at the negative electrode. This trend is most pronounced at 1550°C. In most cases grain growth at the positive electrode and in the center of the sample is very similar. The magnitude of the electric field does not have a strong effect.

In summary, the behavior of the grain growth constant k is very similar to the growth length of single crystals as discussed in section 3.3. However, a gradient in the growth length of the single crystalline seeds was significant only above 1425°C (with faster growth at the negative electrode), but the grain growth constant shows a gradient for all temperatures and fields. It is not clear why the grain size is more sensitive for field induced effects; possibly the electric field increases the driving force for growth of the polycrystal by electrostatic forces as described in the literature [27], but in this case a texture of the grain shape should occur, which was not observed.

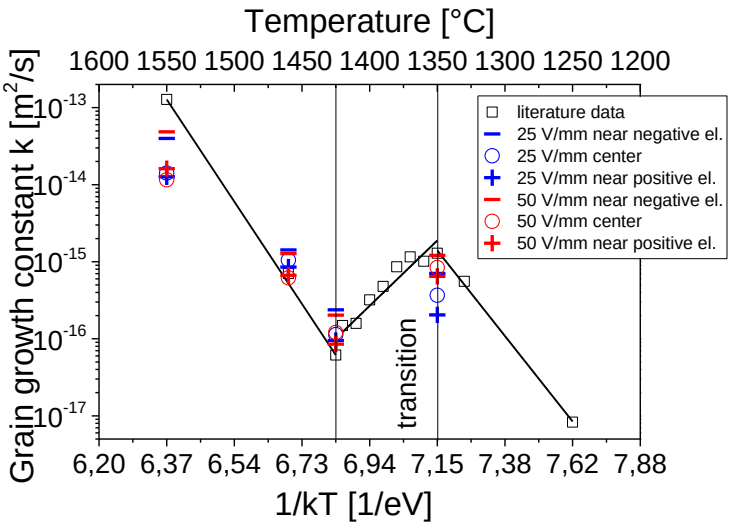

Figure 5: Estimated grain growth constants at the negative electrode, in the center of the sample and at the positive electrode in comparison to literature data [30].

3.5. Impact of defects on grain growth in strontium titanate

The growth effects observed in sections 3.1 and 3.3 can be explained by a defect polarization of the samples. The most important point defects in undoped strontium titanate are oxygen vacancies ($V_O^{\circ\circ}$), electrons (e'), holes (h°) and strontium vacancies (V_{Sr}'') [41]. We propose that a redistribution of these defects causes the gradient in grain boundary mobility in strontium titanate. As discussed in the following, we correlate the local defect concentration and the defect chemistry dependent grain growth behavior of strontium titanate as published in the literature [25, 31, 38, 39, 42].

The defect concentration across the sample is sketched in Figure 6. Electrons and holes are ignored in this graph; their distribution is analogue to strontium and oxygen vacancies, respectively. In the absence of external electric fields the defects are distributed equally in the sample (broken lines in Figure 6). If the material is exposed to an external electric field, the equilibrium defect concentration between the electrodes is changed to the continuous lines with a high concentration of $V_O^{\circ\circ}$ and a low concentration of V_{Sr}'' at the negative electrode (and the inverse at the positive electrode).

The impact of defects (i.e. $V_O^{\circ\circ}$ and V_{Sr}'') was already analyzed in previous studies. The oxygen vacancy concentration was controlled by changing the atmosphere from pure oxygen to reducing atmosphere [25, 36]. Faster grain growth (i.e. a higher grain growth constant k) was observed in reducing atmosphere (i.e. for high $V_O^{\circ\circ}$ concentrations). Several studies focused

on the impact of Strontium vacancies on grain growth at different length scales. Macroscopically, the overall stoichiometry was changed during powder processing. Faster grain growth occurred with excess Strontium in the powder (which accords to a relatively low V_{Sr}'' concentration) [31, 42]. Microscopically, two TEM studies compared the grain boundary mobility with the local defect concentrations at the interfaces. High Ti concentrations (i.e. high V_{Sr}'' concentration) at the boundary were found to be correlated with low grain boundary mobility. Both macroscopic and microscopic observations agree well.

In summary, a high $V_O^{\circ\circ}$ concentration gives high grain boundary mobility whereas high V_{Sr}'' concentrations result in low grain boundary mobility. Given the expected concentration profiles in Figure 6, faster grain growth is expected at the negative electrode. This was observed in experiment as well (cf. Figure 3 and Figure 4). Thus the assumption of a field induced redistribution of defects causing the growth gradients in the samples is plausible.

However, kinetics needs to be addressed [48, 49]. The equilibrium defect profile with external electric field sketched in Figure 6 can only be reached, it the diffusion of defects is fast enough. The diffusion coefficient at 1400°C of $V_O^{\circ\circ}$ is in the order of 10^{-6} cm²/sec [41], the diffusion coefficient of V_{Sr}'' is in the order of 10^{-14} cm²/sec [50]. According to their high mobility, the oxygen vacancies can be assumed to redistribute across the entire sample thickness of 2 mm within minutes [51]. The concentration profile of V_{Sr}'' will need much longer times, possibly the dwell times used in the present experiments is not sufficient for complete redistribution across the sample. But the argumentation above will not change fundamentally, if strontium vacancies do not to reach the proposed equilibrium concentration profile (or even if V_{Sr}'' does not move at all), since the consideration of $V_O^{\circ\circ}$ is sufficient to explain the effects. Unfortunately, the current dataset does not allow estimating kinetics of defect migration; further experiments with intermitted heating times are needed.

Besides of the issue of kinetics, several questions are still open. For example, the defect concentration profile in Figure 6 was sketched according to standard electrochemical models [48, 49, 52]. The exact shape of the profile is not known and most probably more complicated. Figure 4h shows a plateau of the growth length at the positive electrode, while all other data show almost linear gradients across the sample. Possibly this indicates saturation effects of the local defect concentration at high temperatures. Additionally, the

existence of grain boundaries and space charge layers in the polycrystal are ignored completely [53, 54]. Theoretical considerations of the defect concentration profile across the sample and their interplay with local space charge in the polycrystal are highly needed [48, 49]. Additionally, it is not known whether the grain boundary mobility or energy is changed by the local defect concentration, since both are coupled in mean field modelling (i.e. the grain growth constant k).

It should be noted that the defect redistribution shown in Figure 6 results in the formation of an internal electric field, which opposes and compensates the external field. Thus, the sample is field-free. The effect of an electric field on grain growth is not due to the field itself, but due to a change of local defect concentrations by the electric field. The present experimental setup demonstrates the importance of defects in grain growth. If the local defect concentration is calculated by defect chemical equations and under consideration of the electric field, the present experiment is a powerful tool to control defect concentrations continuously and to investigate resulting effects on the material. Other methods as doping and oxygen partial pressure are discontinuous or rather complicated.

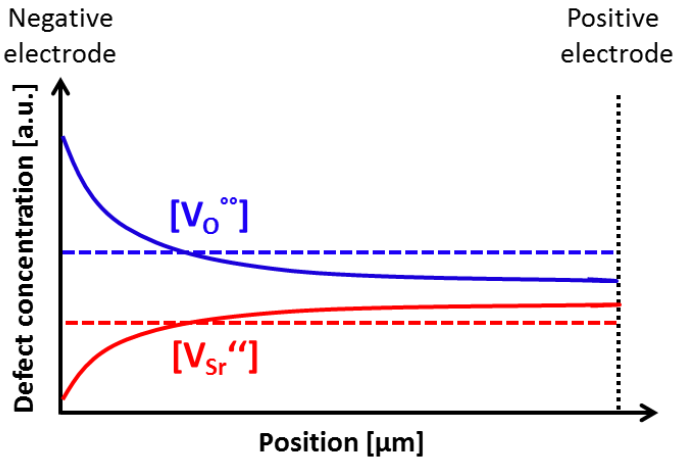

Figure 6: Sketch of the defect redistribution in the samples caused by external electric fields. The upper two lines give the oxygen vacancy ($\mathbf{V_O^{\circ\circ}}$) concentration profile, the lower two lines represent the strontium vacancy ($\mathbf{V_{Sr}''}$) concentration profile. Broke lines give the profiles without external electric field and continuous lines with external electric field.

4. Summary and conclusion

This paper investigates the impact of weak electric fields on grain growth in strontium titanate. To highlight the gradient in grain growth induced by the electric field, the seeded polycrystal technique was chosen: single crystals were diffusion-bonded to polycrystals. The polycrystalline matrix provides a driving force for the single crystal to grow into the polycrystal. The experimental setup used insulating electrodes (alumina) to prevent currents and joule heating. The electric field was parallel to the interface of the single crystal. Thus the field does not change the driving force for the single crystal by electrostatic forces. Two different fields were observed (25 V/mm and 50 V/mm).

The electric field does not have a strong effect on the growth of the single crystalline seeds below 1425°C. Above 1460°C a gradient of the growth length appears with faster growth at the negative electrode. This effect is stronger at higher temperatures and at higher electric fields. The grain growth constant of polycrystals was estimated and agrees well with literature data. Analogue to the growth of the single crystalline seeds, a gradient in the grain growth constant across the sample was found.

The effect of electric fields on grain growth seems to be attributed to defect redistribution across the sample where positive defects (particularly oxygen vacancies) migrate to the negative electrode while negative defects (particularly strontium vacancies) accumulate at the positive electrode. This expected defect concentration profile was connected to defect chemistry dependent grain growth data available in the literature. Since for high oxygen vacancy concentration and low strontium vacancy concentration fast grain growth is expected, the assumed migration of charged defects due to the electric field is in very good accordance to the growth effects observed in this work. However, the details of the defect migration (i.e. kinetics and defect concentration profile) require further theoretical and experimental investigations to quantify the observed correlation between defects and grain growth.

The current experiments demonstrate that even weak electric fields can have a strong effect on grain growth. However, it should be noted that not the electric field itself changes grain growth in strontium titanate, but rather a change of local defect concentrations. The chosen experimental setup provides a powerful tool co correlate grain growth and grain boundary properties to defect chemical parameters.

Acknowledgement

Fruitful discussions with John E. Blendell, Carol A. Handwerker and Suk-Joong L. Kang were highly appreciated.

Appendix

This section gives the derivation of Eqn. 1. The equivalent circuit in Figure 2c shows that the sample is assumed as two capacitors in series. The capacities in this system are

$$C_s = \frac{Q}{U_s} \; and \; C_{tot} = \frac{Q}{U_{tot}} \qquad \text{5a and b}$$

with the capacity of the sample C_s, the insulator C_i and the overall capacity $C_{tot.}$ The charge Q is the same for all capacitors due to the serial circuit. We can combine Eqn. 5a and b to

$$C_s = \frac{C_{tot} U_{tot}}{C_s} \qquad 6$$

The electric field at a dielectric with thickness d is

$$E = \frac{U}{d} \qquad 7$$

and we obtain

$$\frac{E_{sample}}{E_{tot}} = \frac{d_{tot} C_{tot}}{d_s C_s} \qquad 8$$

According to the capacity of a plate capacitor with thickness d_s we obtain the capacity of the sample

$$C_s = \frac{\epsilon_0 \epsilon_{r,STO} A}{d_s} \qquad 9$$

with the permittivity of vacuum ϵ_0, the relative permittivity of strontium titanate $\epsilon_{r,STO}$ and the area of the plates A. The overall capacity of the sample setup is

$$C_{tot} = \frac{1}{\frac{1}{C_s} + \frac{1}{C_i}} \qquad 10$$

Combining Eqns. 8, 9 and 10 we obtain Eqn. 1:

$$\frac{E_{sample}}{E_{tot}} = \frac{d_s + d_i}{d_s \left(1 + \frac{\epsilon_{r,STO} d_i}{\epsilon_{r,alumina} d_s}\right)} \qquad 1$$

with $\epsilon_{r,alumina}$ as the relative permittivity of alumina and d_i as the thickness of both alumina plates.

References

[1] R. Raj, M. Cologna, and J. S. C. Francis, "Influence of externally imposed and internally generated electrical fields on grain growth, diffusional creep, sintering and related phenomena in ceramics," *J. Am. Ceram. Soc.*, vol. 94, pp. 1941–1965, JUL 2011.

[2] J. Narayan, "A new mechanism for field-assisted processing and flash sintering of materials," *Scr. Mater.*, vol. 69, pp. 107–111, July 2013.

[3] M. Cologna, J. S. C. Francis, and R. Raj, "Field assisted and flash sintering of alumina and its relationship to conductivity and mgo-doping," *J. Eur. Ceram. Soc.*, vol. 31, no. 15, pp. 2827–2837, 2011.

[4] E. Zapata-Solvas, S. Bonilla, P. R. Wilshaw, and R. I. Todd, "Preliminary investigation of flash sintering of SiC," *J. Eur. Ceram. Soc.*, vol. 33, pp. 2811–2816, Nov. 2013.

[5] J. S. C. Francis, M. Cologna, and R. Raj, "Particle size effects in flash sintering," *J. Eur. Ceram. Soc.*, vol. 32, pp. 3129–3136, Sept. 2012.

[6] J. A. Downs and V. M. Sglavo, "Electric field assisted sintering of cubic zirconia at 390 degrees C," *J. Am. Ceram. Soc.*, vol. 96, pp. 1342–1344, May 2013.

[7] R. Baraki, S. Schwarz, and O. Guillon, "Effect of electrical field/current on sintering of fully stabilized zirconia," *J. Am. Ceram. Soc.*, vol. 95, pp. 75–78, JAN 2012.

[8] M. Cologna, B. Rashkova, and R. Raj, "Flash sintering of nanograin zirconia in < 5 s at 850 degrees C," *J. Am. Ceram. Soc.*, vol. 93, pp. 3556–3559, Nov. 2010.

[9] S.-W. Kim, S.-J. L. Kang, and I.-W. Chen, "Electro-sintering of yttria-stabilized cubic zirconia," *J. Am. Ceram. Soc.*, vol. 96, pp. 1398–1406, May 2013.

[10] J. C. M'Peko, J. S. C. Francis, and R. Raj, "Field-assisted sintering of undoped $BaTiO_3$: Microstructure evolution and dielectric permittivity," *J. Eur. Ceram. Soc.*, vol. 34, pp. 3655–3660, Dec. 2014.

[11] A. Karakuscu, M. Cologna, D. Yarotski, J. Won, J. S. C. Francis, R. Raj, and B. P. Uberuaga, "Defect structure of flash-sintered strontium titanate," *J. Am. Ceram. Soc.*, vol. 95, pp. 2531–2536, Aug. 2012.

[12] J. Park and I.-W. Chen, "In situ thermometry measuring temperature flashes exceeding 1,700 degrees C in 8 mol% Y_2O_3-stablized zirconia under constant-voltage heating," *J. Am. Ceram. Soc.*, vol. 96, pp. 697–700, Mar. 2013.

[13] S. Grasso, Y. Sakka, N. Rendtorff, C. Hu, G. Maizza, H. Borodianska, and O. Vasylkiv, "Modeling of the temperature distribution of flash sintered zirconia," *J. Ceram. Soc. Jpn.*, vol. 119, pp. 144–146, Feb. 2011.

[14] R. Raj, "Joule heating during flash-sintering," *J. Eur. Ceram. Soc.*, vol. 32, pp. 2293–2301, Aug. 2012.

[15] J. Narayan, "Grain growth model for electric field-assisted processing and flash sintering of materials," *Scr. Mater.*, vol. 68, pp. 785–788, May 2013.

[16] D. Yang, R. Raj, and H. Conrad, "Enhanced sintering rate of zirconia (3Y-TZP) through the effect of a weak dc electric field on grain growth," *J. Am. Ceram. Soc.*, vol. 93, no. 10, pp. 2935–2937, 2010.

[17] S. Ghosh, A. H. Chokshi, P. Lee, and R. Raj, "A huge effect of weak DC electrical fields on grain growth in zirconia," *J. Am. Ceram. Soc.*, vol. 92, no. 8, pp. 1856–1859, 2009.

[18] J. W. Cahn, "Impurity-drag effect in grain boundary motion," *Acta Metallurgica*, vol. 10, p. 789, 1962.

[19] H. R. Jin, S. H. Yoon, J. H. Lee, J. H. Lee, N. M. Hwang, D. Y. Kim, and J. H. Han, "Effect of external electric field on the grain-growth behavior of barium titanate," *J. Am. Ceram. Soc.*, vol. 87, pp. 1747–1752, Sept. 2004.

[20] H. R. Jin, S. H. Yoon, J. H. Lee, N. M. Hwang, D. Y. Kim, and J. H. Han, "Effect of external electric field on the grain growth of barium titanate in N_2 atmosphere," *Journal of Materials Science-materials In Electronics*, vol. 16, pp. 749–752, Nov. 2005.

[21] Y.-I. Jung, S.-Y. Choi, and S.-J. L. Kang, "Effect of oxygen partial pressure on grain boundary structure and grain growth behavior in $BaTiO_3$," *Acta Mater.*, vol. 54, pp. 2849–2855, 2006.

[22] B.-K. Lee, S.-Y. Chung, and S.-J. Kang, "Grain boundary faceting and abnormal grain growth in $BaTiO_3$," *Acta Mater.*, vol. 48, pp. 1575–1580, 2000.

[23] B. K. Lee and S.-J. L. Kang, "Second-phase assisted formation of 111 twins in barium titanate," *Acta Mater.*, vol. 49, no. 8, pp. 1373–1381, 2001.

[24] S. Y. Choi and S. J. L. Kang, "Control of boundary structure and grain growth for microstructural design," *Pricm 5: the Fifth Pacific Rim International Conference On Advanced Materials and Processing, Pts 1-5*, vol. 475-479, pp. Chinese Soc Met; Japan Inst Met; Korea Inst Met & Mat; Minerals, Met &EOLEOLMat Soc, 2005.

[25] W. Rheinheimer, M. Bäurer, and M. J. Hoffmann, “A reversible wetting transition in strontium titanate and its influence on grain growth and the grain boundary mobility,” *Acta Mater.*, vol. 101, pp. 80–89, 05 2015.

[26] W. Rheinheimer, M. Bäurer, C. A. Handwerker, J. E. Blendell, and M. J. Hoffmann, “Growth of single crystalline seeds into polycrystalline strontium titanate: Anisotropy of the mobility, intrinsic drag effects and kinetic shape of grain boundaries,” *Acta Materialia*, vol. 95, no. 0, pp. 111 – 123, 2015.

[27] J. W. Jeong, J. H. Han, and D. Y. Kim, “Effect of electric field on the migration of grain boundaries in alumina,” *J. Am. Ceram. Soc.*, vol. 83, pp. 915–918, Apr. 2000.

[28] M. Kinoshita, “Boundary migration of single crystal in polycrystalline alumina,” *Yogyo Kyokai Shi*, vol. 82, no. 5, pp. 295–296, 1974.

[29] L. Amaral, M. Fernandes, I. M. Reaney, M. P. Harmer, A. M. R. Senos, and P. M. Vilarinho, “Grain growth anomaly and dielectric response in Ti-rich strontium titanate ceramics,” *The Journal of Physical Chemistry*, vol. 117, p. 24787?24795, 2013.

[30] W. Rheinheimer and M. J. Hoffmann, “Non-arrhenius behavior of grain growth in strontium titanate: New evidence for a structural transition of grain boundaries,” *Scr. Mater.*, vol. 101, pp. 68–71, May 2015.

[31] M. Bäurer, D. Weygand, P. Gumbsch, and M. J. Hoffmann, “Grain growth anomaly in strontium titanate,” *Scr. Mater.*, vol. 61, no. 6, p. 584–587, 2009.

[32] T. Sano, D. M. Saylor, and G. S. Rohrer, “Surface energy anisotropy of $SrTiO_3$ at 1400°C in air,” *J. Am. Ceram. Soc.*, vol. 86, no. 11, pp. 1933–1939, 2003.

[33] W. Rheinheimer, M. Bäurer, H. Chien, G. S. Rohrer, C. A. Handwerker, J. E. Blendell, and M. J. Hoffmann, “The equilibrium crystal shape of strontium titanate and its relationship to the grain boundary plane distribution,” *Acta Mat.*, vol. 82, pp. 32–40, 2015.

[34] D. M. Saylor, B. El-Dasher, T. Sano, and G. S. Rohrer, “Distribution of grain boundaries in $SrTiO_3$ as a function of five macroscopic parameters,” *J. Am. Ceram. Soc.*, vol. 87, no. 4, pp. 670–676, 2004.

[35] M. Syha, W. Rheinheimer, M. Bäurer, E. M. Lauridsen, W. Ludwig, D. Weygand, and P. Gumbsch, “Three-dimensional grain structure of sintered bulk strontium titanate from X-ray diffraction contrast tomography,” *Scr. Mater.*, vol. 66, no. 1, pp. 1–4, 2012.

[36] S.-Y. Chung, D. Y. Yoon, and S.-J. L. Kang, “Effects of donor concentration and oxygen partial pressure on interface morphology and grain growth behavior in $SrTiO_3$,” *Acta Mater.*, vol. 50, pp. 3361–3371, 2002.

[37] H. Sternlicht, W. Rheinheimer, M. J. Hoffmann, and W. D. Kaplan, “The mechanism of grain boundary motion in $SrTiO_3$,” *J. Mater. Sci.*, vol. 51, pp. 1–9, 2015. In press.

[38] M. Bäurer, S.-J. Shih, C. Bishop, M. P. Harmer, D. Cockayne, and M. J. Hoffmann, “Abnormal grain growth in undoped strontium and barium titanate,” *Acta Mater.*, vol. 58, pp. 290–300, 2010.

[39] S.-J. Shih, S. Lozano-Perez, and D. J. H. Cockayne, “Investigation of grain boundaries for abnormal grain growth in polycrystalline $SrTiO_3$,” *J. Mater. Res.*, vol. 25, no. 2, pp. 260–265, 2010.

[40] N. Shomrat, D. Haviv, and Y. Tsur, “The correlation between non-stoichiometry and charge compensation in perovskites,” *Journal of Electroceramics*, vol. 33, pp. 135–141, 2014.

[41] R. Moos and K. Härdtl, “Defect chemistry of donor-doped and undoped strontium titanate ceramics between 1000°C and 1400°C,” *J. Am. Ceram. Soc.*, vol. 80, no. 10, pp. 2549–2562, 1997.

[42] M. Bäurer, H. Kungl, and M. J. Hoffmann, “Influence of Sr/Ti stoichiometry on the densification behavior of strontium titanate,” *J. Am. Ceram. Soc.*, vol. 92, pp. 601–606, 2009.

[43] J. V. FLORIO, “Dielectric properties of alumina at high temperatures,” *Journal of the American Ceramic Society*, vol. 43, no. 5, pp. 262–267, 1960.

[44] M. Vollman and R. Waser, “Grain boundary defect chemistry of acceptor-doped titanates: Space charge layer width,” *J. Am. Ceram. Soc.*, vol. 77, no. 1, pp. 235–243, 1994.

[45] W. Rheinheimer and M. Hoffmann, “Grain growth transitions of perovskite ceramics and their relationship to abnormal grain growth and bimodal microstructures,” *Journal of Materials Science*, vol. HTC 2015, pp. 1–10, 2015.

[46] W. Rheinheimer and M. Hoffmann, “Grain growth in perovskites: What is the impact of boundary transitions?.” submitted to Current Opinion in Solid State and Materials Science, 2015.

[47] J. E. Burke and D. Turnbull, “Recrystallization and grain growth,” *Progress in Metal Physics*, vol. 3, pp. 220–292, 1952.

[48] R. A. De Souza, “Oxygen diffusion in $SrTiO_3$ and related perovskite oxides,” *Advanced Functional Materials*, vol. 25, pp. 6326–6342, Oct. 2015.

[49] R. A. De Souza, V. Metlenko, D. Park, and T. E. Weirich, “Behavior of oxygen vacancies in single-crystal $SrTiO_3$: Equilibrium distribution and diffusion kinetics,” *Physical Review B*, vol. 85, p. 174109, May 2012.

[50] R. Meyer, R. Waser, J. Helmbold, and G. Borchardt, “Observation of vacancy defect migration in the cation sublattice of complex oxides by 18O tracer experiments,” *Phys. Rev. Lett.*, vol. 90, no. 10, p. 105901, 2003.

[51] P. Paul C. McIntyre, “Point defect equilibrium in strontium titanate thin films,” *J. Appl. Phys.*, vol. 89/12, pp. 8074–8084, 2001.

[52] A. J. Moulson and J. M. Herbert, *Electroceramics : materials, properties, applications*. Chichester: Wiley, 2. ed. ed., 2003. Includes bibliographical references and index.

[53] Y.-M. Chiang and T. Takagi, “Grain-boundary chemistry of barium titanate and strontium titanate: I, high-temperature equilibrium space charge,” *J. Am. Ceram. Soc.*, vol. 73, no. 11, pp. 3278–3285, 1990.

[54] Y.-M. Chiang and T. Takagi, “Grain-boundary chemistry of barium titanate and strontium titanate: II, origin of electrical barriers in positive-temperature-coefficient thermistors,” *J. Am. Ceram. Soc.*, vol. 73, pp. 3286–3291, 1990.